Impact of trailing edge shape on the wake and propulsive performance of pitching panels

T. Van Buren, D. Floryan, D. Brunner, U. Senturk, and A. J. Smits

Phys. Rev. Fluids **2**, 014702 — Published 9 January 2017

DOI: 10.1103/PhysRevFluids.2.014702

Impact of trailing edge shape on the wake and propulsive performance of pitching panels

T. Van Buren,[1, a)] D. Floryan,[1] D. Brunner,[2] U. Senturk,[3] and A.J. Smits[1, 4]

[1)] *Mechanical and Aerospace Engineering, Princeton University,Princeton NJ 08544, USA*

[2)] *School of Engineering, Zurich University of Applied Sciences, 8401 Winterthur, Switzerland*

[3)] *Department of Mechanical Engineering, Ege University, Izmir 35040, Turkey*

[4)] *Department of Mechanical and Aerospace Engineering, Monash University, VIC 3800, Australia*

The effects of changing the trailing edge shape on the wake and propulsive performance of a pitching rigid panel are examined experimentally. The panel aspect ratio is $AR = 1$, and the trailing edges are symmetric chevron shapes with convex and concave orientations of varying degree. Concave trailing edges delay the natural vortex bending and compression of the wake, and the mean streamwise velocity field contains a single jet. Conversely, convex trailing edges promote wake compression and produce a quadfurcated wake with four jets. As the trailing edge shape changes from the most concave to the most convex, the thrust and efficiency increase significantly.

[a)] Email address for correspondence: tburen@princeton.edu

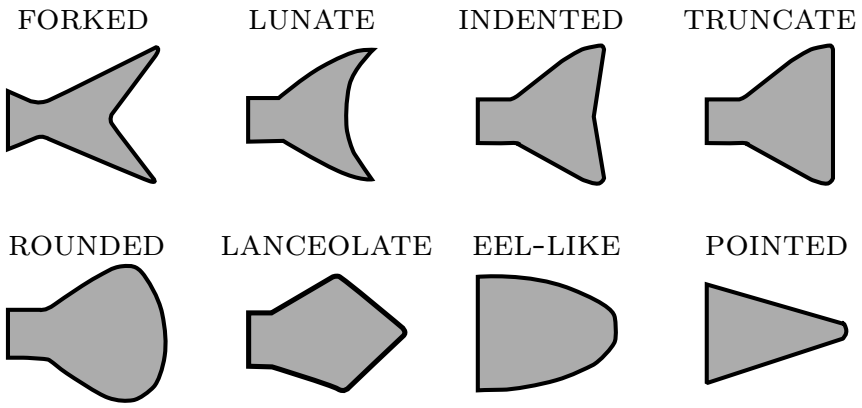

FIG. 1: The variety of fish caudal fin types (various sources).

I. INTRODUCTION

Many aquatic animals swim by oscillating their caudal fins, and these fins have evolved to exhibit a wide range of shapes[1]. The shapes may be described as concave, where the trailing edge is indented to some degree (e.g., forked pike tail), square, where the trailing edge is straight (e.g., truncated trout tail), or convex, where the trailing edge is protruding (e.g., eel-like tails), as shown in figure 1.

The shape of the caudal fin has been observed to affect the fish swimming efficiency, acceleration, and maneuverability[2,3]. To better understand the effects on performance, a number of investigations have systematically altered the planform of fin-like propulsors. For example, Karpouzian, Spedding, and Cheng[4] analytically compared the performance of fins with varying aspect ratio and sweep, and both parameters were found to have a significant impact on thrust and efficiency. The effects of sweep as it applies to many fish-like propulsors were studied numerically by Chopra[5] and Li, Luodin, and Lu[6], and Liu and Bose[7] compared the performance of three whale fins using a quasi-vortex-lattice numerical method. By varying pitch and heave amplitude, it was found that the tail shape significantly altered the conditions for maximum efficiency. Lauder *et al.*[8] isolated the effects of trailing edge shape for highly flexible panels of very low aspect ratio ($0.194 \leq AR \leq 0.340$) akin to eel-like swimmers, and found experimentally that the trailing edge could be manipulated to improve the panel self-propelled swimming speed. The aspect ratio is given by $AR = S/c$, where S is the span and c is the chord length. In all these studies, however, more than one fin parameter was changed at the same time. For example, changing the sweep alters the

angle of the leading and trailing edges simultaneously, and changing the planform of the panel also affects its flexibility.

Here, we focus on the effects of only changing the trailing edge shape on the wake and performance of a pitching panel. Based on previous work on pitching panels with square trailing edges, we expect that the trailing edge shape will have a significant impact on the vortex dynamics and stability of the wake. Low aspect ratio fins ($AR = O(1)$), representative of what is seen in biology, yield highly three-dimensional wakes. Even for a simple rectangular panel in pitching motion, the structure of the wake depends on many factors. In its simplest form, a so-called 2S wake is formed, where each swimming stroke sheds a vortex loop from the trailing edge that convects downstream, so that on the midspan the wake appears as a reverse von Kármán vortex street. For a pitching panel with $AR = 0.54$, Buchholz and Smits [9] demonstrated that the wake formation is dominated by the streamwise vorticity generated at the panel edges, driving the wake towards the panel center, very much like the axis switching phenomena of non-axisymmetric jets (Dhanak and Bernardinis [10]). This compression in the spanwise direction is coupled with spreading in the panel-normal direction, and as the Strouhal number increases the wake splits into two jets each formed by a pair of vortices, marking the transition from a 2S to a 2P wake. The Strouhal St number is defined by $St = fa/U_\infty$, where f is the actuation frequency, a is the characteristic width of the wake (often represented by the amplitude of the trailing edge motion), and U_∞ is the freestream velocity (equal to the swimming speed if the foil were allowed to move freely). Green, Rowley, and Smits [11] observed a similar behavior for low aspect ratio trapezoidal panels with square trailing edges.

No similar study has been reported with non-square trailing edges, and so we investigate the effects of varying the trailing edge shape by using concave and convex chevron-shaped trailing edges, and compare the three-dimensional wake evolution and performance to the baseline square panel case. We examine the wake evolution using particle image velocimetry (PIV), and the performance by measuring the thrust T, and the propulsive efficiency $\eta = TU_\infty/P$, where $P = T_z\,\dot{\theta}$ is the power input to the flow, T_z is the spanwise torque, and $\dot{\theta}$ is the angular velocity of pitching.

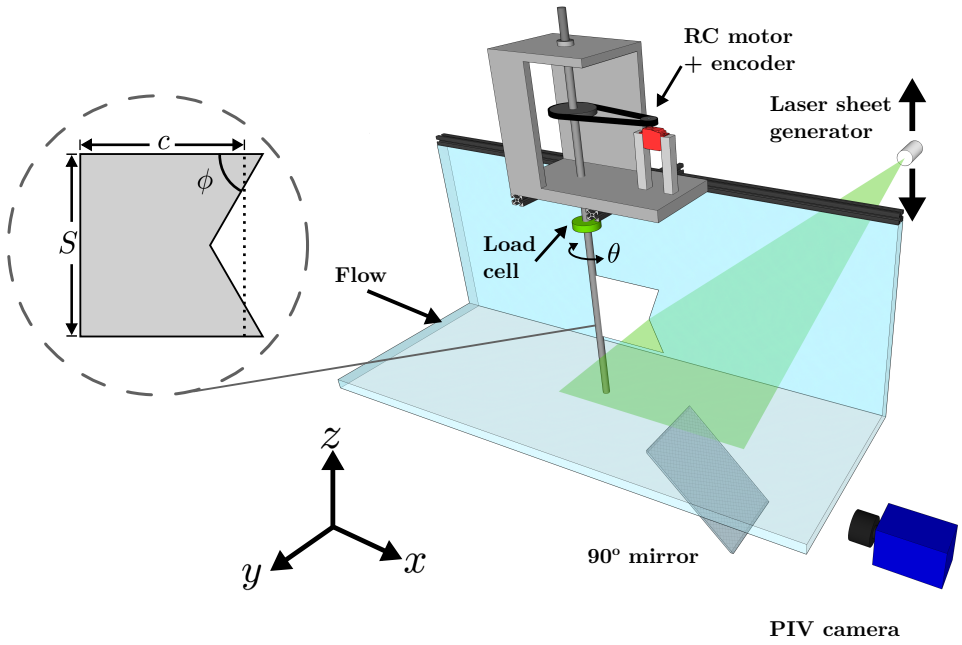

FIG. 2: Experimental setup.

II. EXPERIMENTAL METHODS

Experiments were conducted on rigid panels, pitching about the leading edge, in a free-surface recirculating water channel facility. A schematic of the experiment showing the plate geometries is given in figure 2. The panel trailing edge corner angles were varied from $\phi = 45°$ to $135°$ in intervals of $15°$, with $\phi = 90°$ corresponding to a square panel. All other panel properties were matched, including surface area, $A = 100$ cm^2; mean chord, $c = 10$ cm; span $S = 10$ cm; and mean aspect ratio, $AR = 1$. The freestream velocity was fixed at $U_\infty = 6.0$ cm/s for the wake analysis and $U_\infty = 10.0$ cm/s for the performance measurements, corresponding to chord based Reynolds numbers of $Re = 6000$ and $Re = 10,000$, respectively. Peak turbulence intensities were 0.8% and a plate was mounted at the free surface to suppress waves.

The pitching amplitude was varied from $\theta = 9°$ to $15°$ in intervals of $3°$, and the frequency of the sinusoidal actuation was varied from $f = 0.5$ to 2 in intervals of 0.15 Hz. All combinations of pitch amplitudes and frequencies in these ranges were tested, corresponding to a Strouhal number range of $St = 0.16$ to 1 ($a = 2\,c\,\sin\theta$). Wake measurements were limited to the Strouhal number corresponding to free swimming, $St = 0.2$, which is the condition

where there was no net force acting on the panel. Performance measurements covered the entire Strouhal number range.

Two-component particle image velocimetry (PIV) was used to analyze the flow field surrounding the panel. The flow was seeded using neutrally buoyant silver coated hollow ceramic spheres (Potter Industries Inc. Conduct-O-Fil AGSL150 TRD) and was illuminated in a plane centered on the panels using a CW argon-ion laser (Spectra Physics 2020). Images were taken by a 8-bit monochrome CCD camera (MotionXtra HG-LE) with 1128×752 resolution. The image acquisition frequency was fixed at 25 Hz, sufficient for time-resolved measurements, and a minimum of 10 actuation periods were sampled for the purposes of phase-averaging. Images were processed sequentially using commercial DaVis software, where local spatial correlations were computed once at interrogation window sizes of 64×64 and twice at 32×32 with 50% overlap. Multiple windows were stitched together in post-processing to produce the full vector field with a grid size of 70×47 velocity vectors. The average and instantaneous velocity errors are estimated to be 2.7% and 1-5%, respectively (Sciacchitano, Wieneke, and Scarano[12]). Interrogation planes were spaced every 5 mm along the half-span of the panel and mirrored to construct a volume. A three-dimensional flow volume is constructed, but it is limited to the x- and y-components of velocity (streamwise U and panel-normal V) and the z-component of vorticity (ω_z, spanwise).

Hydrogen bubble flow visualization[13] provided qualitative analysis of the vortex dynamics. Hydrogen bubbles were created using a 25 μm diameter tungsten wire anode and a brass plate cathode with a charge of ∼40 volts. The bubble generating wire was oriented in the spanwise direction and placed near the trailing edge of the pitching panel. A camera (Nikon D7000) was used to acquire 1920 × 1080 pixel resolution video at 24 frames per second. Twenty oscillation periods were acquired and phase averaged with background subtraction for the final images.

The thrust and power were measured with a six-component force and torque sensor (ATI Mini40), which has force and torque resolutions of 5×10^{-3} N and 1.25×10^{-4} Nm in the x- and y-directions. The frequency response of the sensor was about 100 Hz, permitting time-resolved measurements. A total of 20 periods were used to calculate time-averaged quantities, and each case was run three times independently to verify repeatability and provide a quantitative measure of uncertainty.

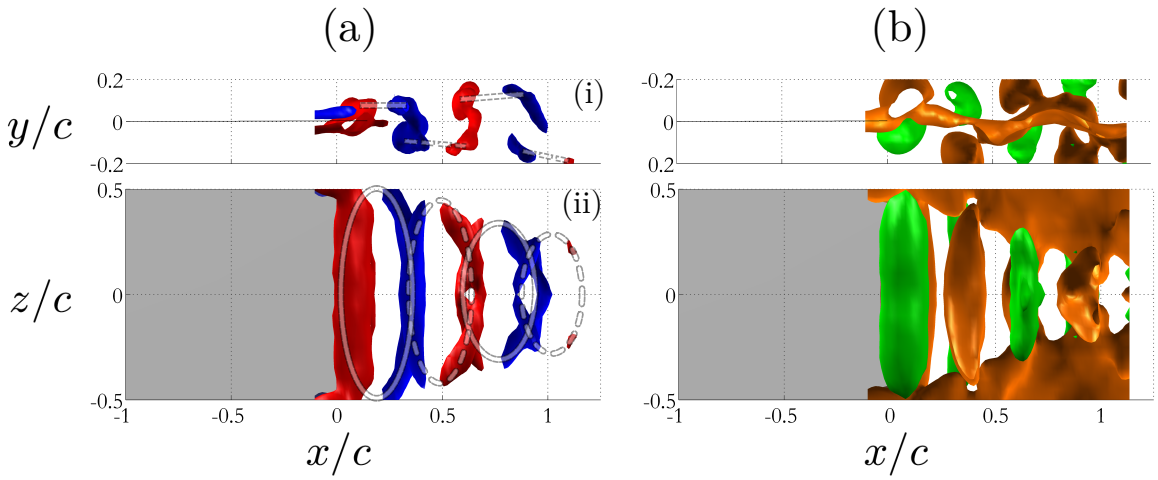

FIG. 3: Square trailing edge panel isosurfaces of phase-averaged (a) spanwise vorticity $\langle\omega_z^*\rangle$ (red is positive and blue is negative) and (b) streamwise velocity ($\langle U\rangle/U_\infty = 0.9$, orange; $\langle U\rangle/U_\infty = 1.1$, green) obtained for $St = 0.2$, $AR = 1$, $Re = 6000$. Spanwise (i) and panel-normal (ii) views are shown for each case. The panel is moving into the negative y domain (phase angle 180°). Flow is from left to right.

III. RESULTS

We begin by exploring the square panel wake. Figure 3a shows the phase-averaged isosurfaces of the spanwise vorticity, using thresholds of $\omega_z^* = \pm 1.0 \times 10^{-3}$ where $\omega_z^* = \omega_z c/U_\infty$. The wake is marked by a train of vortex loops, indicated using solid and dashed lines overlaid on the vortex structure for clarity. The vortex at the trailing edge starts aligned in the spanwise direction, corresponding to the trailing edge orientation, then bends outward as it develops due to the induced velocity of the neighboring vortices compressing the wake in the spanwise direction and expanding it in the panel-normal direction. This matches the behavior seen by Buchholz and Smits[9] and Green, Rowley, and Smits[11] for square trailing-edged panels in pitching motion.

Isosurfaces of the phase-averaged streamwise velocity for the same square panel are depicted in figure 3b, showing regions of higher (+10%) and lower (−10%) velocity with respect to the freestream velocity. The regions of higher and lower velocity oriented in the spanwise directions correspond to the spanwise vortices, but there is also a large and growing region of decelerated flow originating at each panel edge, which appear as a snake-like structure in

the top view. Such regions appear because of the virtual blockage created by the spanwise flow on the panel due to the limited aspect ratio of the panel.

A. Effects of trailing edge shape on the wake

Changing the trailing edge shape has a marked influence on the alignment of the vortices in the wake. Figure 4 shows that for a concave trailing edge the vortex starts bent inwards, opposite to the natural bending direction, causing the vortex to remain oriented in the spanwise direction for a longer distance than for the square panel. This also restricts the wake compression. Conversely, for a convex trailing edge the vortex is initially bent outwards and then continues to bend and lose coherence more quickly than for the other cases. The wake compression appears to be enhanced in this case. These effects increase with corner angle for both concave and convex panels. With the limitations of still images it can be difficult to understand the vortex structure dynamics. Please refer to the supplemental videos for an improved perception of the flow field.

To examine the mean streamwise momentum associated with the wake, the isosurfaces of the time-averaged streamwise velocity $\overline{U}/U_\infty$ are shown in figure 5 for $\phi = 60°$, $90°$, and $120°$. The remaining panels with a more limited field of view are shown in figure 6. For each panel there are regions of accelerated and decelerated flow relative to the free stream. The edges of the panels produce regions of low streamwise velocity in all cases because the vortices produced by the edges of the panel impede the oncoming flow, exerting a virtual blockage on the streamwise velocity. For the concave trailing edge the region of acceleration is a single jet, with lower velocity regions in the wake of the panel edges. The square panel starts as a single jet-like wake, but then splits further downstream. The convex panel has a much different mean streamwise momentum distribution, where the high velocity region has quadfurcated (split into four parts), and the lower velocity region exists throughout the entire span of the panel downstream. This quadfurcation is an artifact of time-averaging. It is important to remember that this is a time-average of a periodic flow, so these results do not represent an instantaneous view of the wake of the panel. The phase-averaged velocity fields portray an instantaneous snapshot of the wake, shown in figure 7. Here the region of higher velocity splits in the spanwise direction, which is why we see the quadfurcation in the time-averaged figures. This is especially notable for $\phi = 105°$, $120°$, and $135°$.

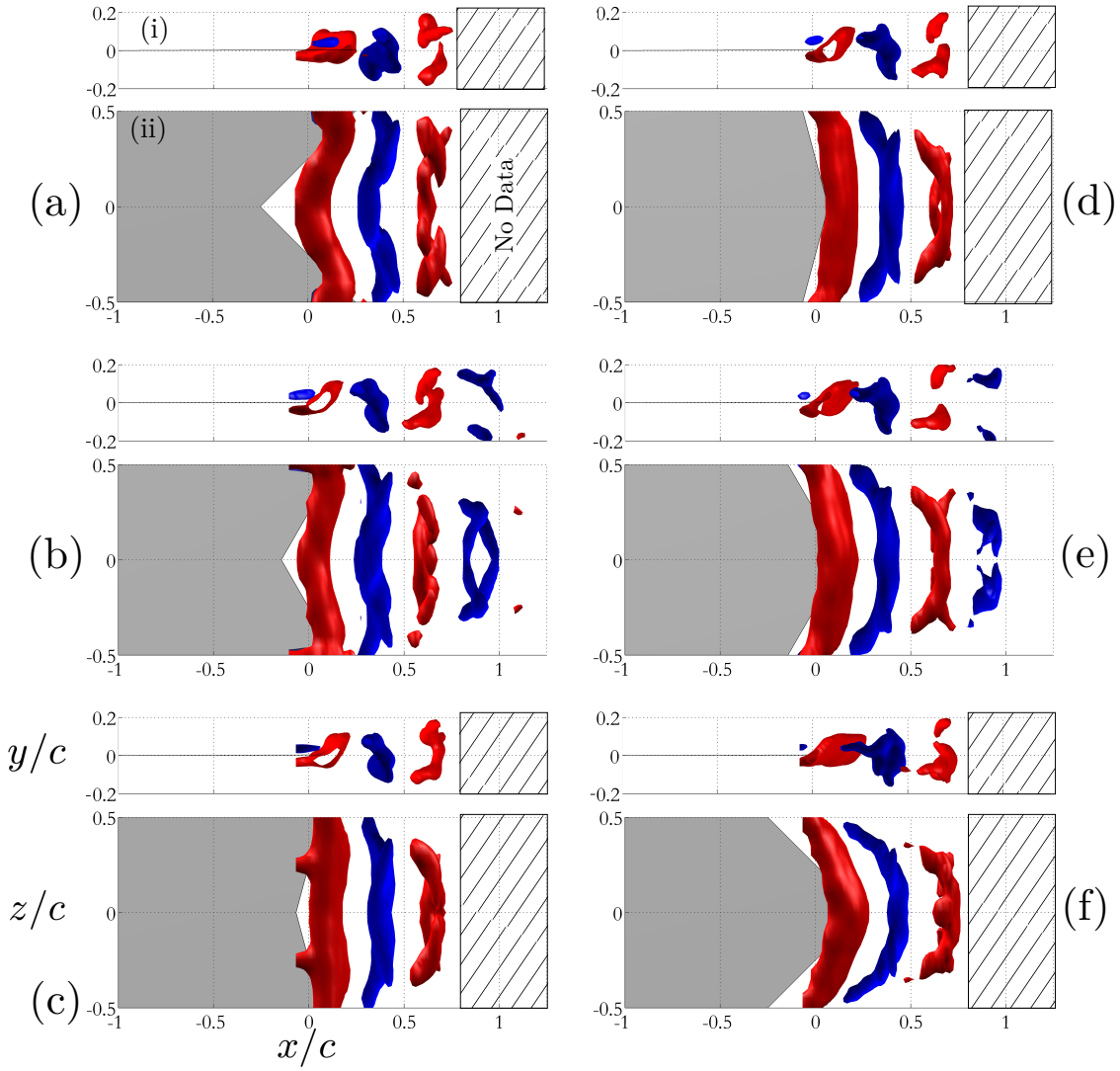

FIG. 4: Isosurfaces of phase-averaged spanwise vorticity $\langle \omega_z^* \rangle$, for $St = 0.2$. Red is positive, blue is negative. Spanwise and panel-normal views are shown for each case. (a) $\phi = 45°$; (b) 60°; (c) 75°; (d) 105°; (e) 120°; (f) 135°. The panel is moving into the negative y domain (phase angle 180°). Videos of the phase-averaged vortex time evolution for $\phi = 60°$, 90°, and 120° are available online (link to be added).

Given the limitations of isosurfaces in describing flow behavior, and that only a single component of vorticity was measured, we used hydrogen bubble flow visualization to augment the PIV data. Figure 8 shows a phase-averaged image of the wakes generated by concave, square, and convex panels. All cases are for $St = 0.2$, but for different combinations of pitch

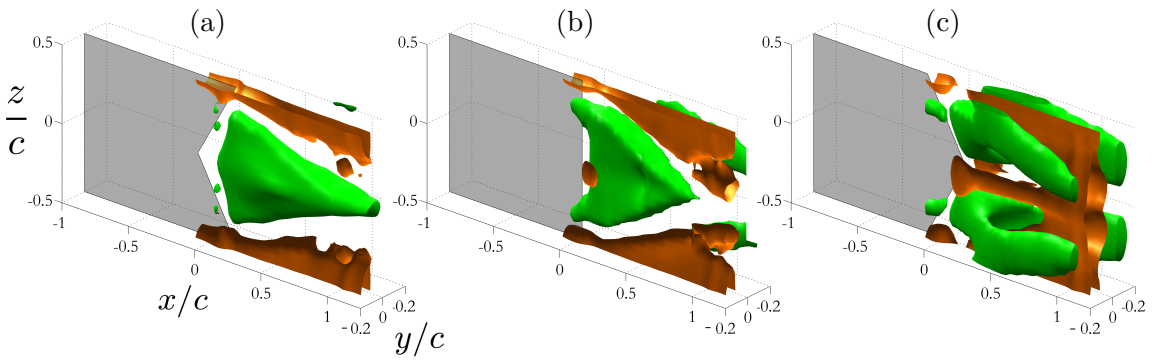

FIG. 5: Isosurfaces of time-averaged of streamwise velocity $\overline{U}/U_\infty$ thresholded at 0.92 (orange) and 1.03 (green), for $St = 0.2$. (a) $\phi = 60°$; (b) 90°; (c) 120°. See also figure 6.

angle and reduced frequency ($k = 2\pi fc/U_\infty$). The flow field is similar to what was depicted by the isosurface vorticity plots in figures 3 and 4, in that the trailing edge vortex shape is dictated by the trailing edge angle, and the vortex shape influences the extent of the wake coherence. Also, the wake is relatively robust to changes in frequency and pitch amplitude for matched Strouhal numbers.

The spanwise splitting of the wake discussed with respect to figure 7 for $\phi = 105°$, 120°, and 135° is seen most clearly in the flow visualizations for the cases given in figure 8.c. The Strouhal number is constant, but we see the splitting became more evident as the frequency increases. This splitting phenomenon, therefore, may not be governed by Strouhal number alone, and reduced frequency may also be an important parameter.

In summary, the three-dimensional wake characteristics of these low aspect ratio panels are characterized by a train of non-axisymmetric vortex rings, which undergo axis switching and cause the wake to compress in the spanwise direction and expand in the panel-normal direction. Changing the trailing edge shape changes the shape of the trailing edge vortex, thereby modifying the subsequent vortex interactions. For the concave trailing edges ($\phi \geq 105°$) it appears that the vortex rings meet and pinch off[10], causing the wake to split in the spanwise direction. This behavior has also been seen in trapezoidal panels[14].

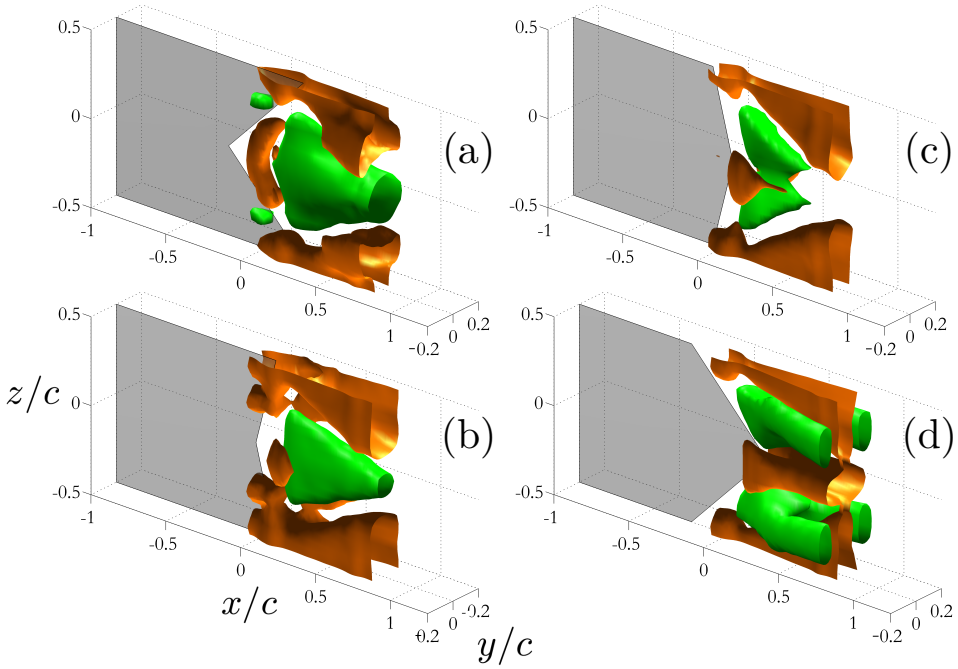

FIG. 6: Isosurfaces of time-averaged of streamwise velocity $\overline{U}/U_\infty$ thresholded at 0.92 (orange) and 1.03 (green), for $St = 0.2$. (a) $\phi = 45°$; (b) 75°; (c) 105°; (d)135°.

B. Effects of trailing edge shape on performance

Figure 9 presents the thrust coefficients, $C_T = T/(\frac{1}{2}\rho U_\infty^2 Sc)$ where ρ is the fluid density, for a range of Strouhal numbers. The uncertainty bars are smaller than the symbols. For all panels the thrust increases with Strouhal number, with the zero-thrust free-swimming condition occurring at $St \sim 0.2$. The change in thrust relative to the square panel, ΔC_T, is shown in figure 9(b). These differences were obtained from a curve fit to the data so as to minimize experimental scatter. For all cases we see a clear trend of increasing thrust with panel trailing edge angle for a given Strouhal number, with the most convex panel producing a thrust that is about 15% higher than the square panel. This change in the thrust is accompanied by a transition from a single jet-like wake for the concave panels to the quadfurcated wake for the convex panels.

The propulsive efficiency is shown in figure 10 for the same range of Strouhal numbers where the uncertainty bars represent measurement repeatability. The efficiency generally increases rapidly up to a peak around $0.38 \leq St \leq 0.42$, and then gradually decreases with

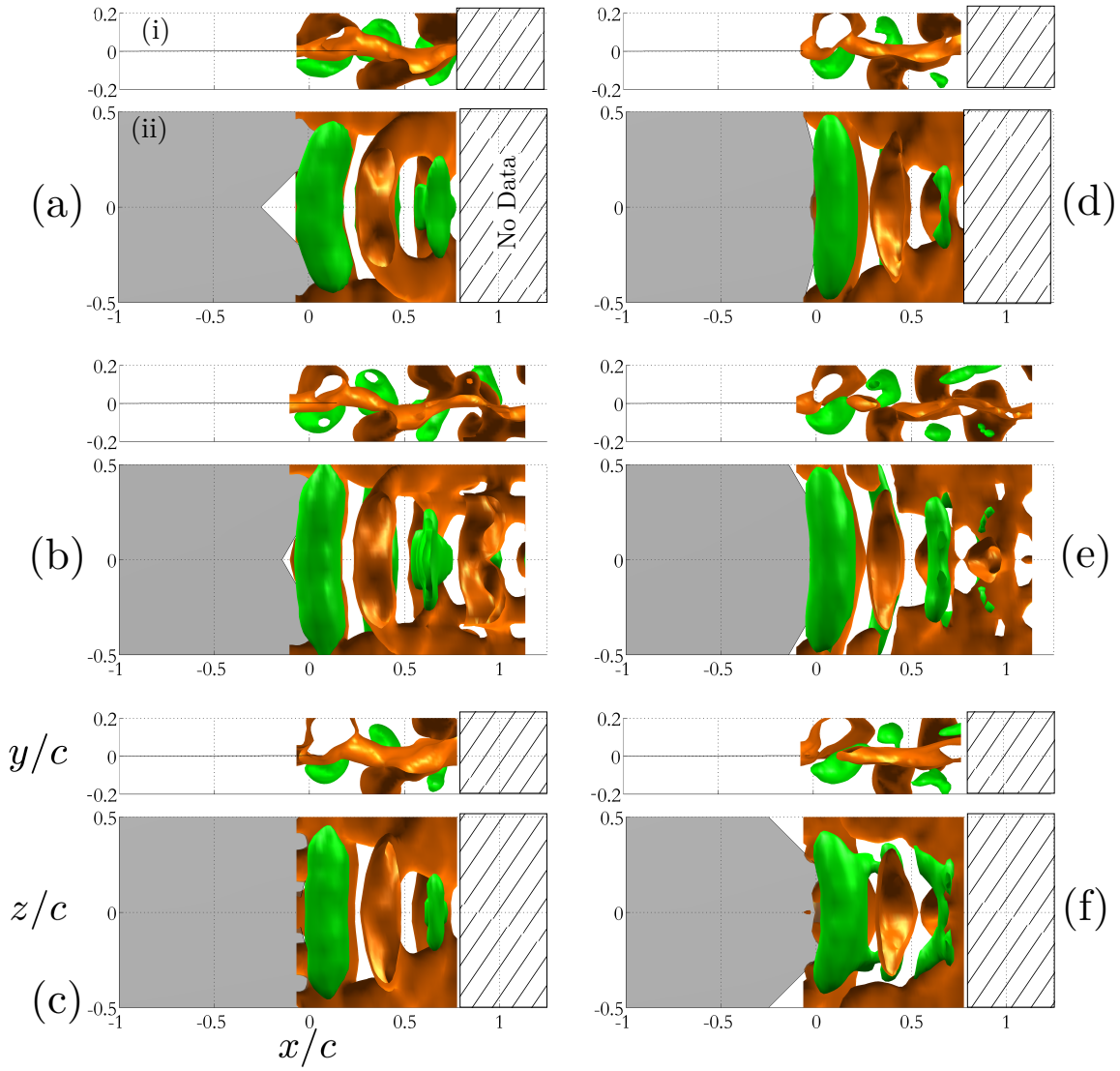

FIG. 7: Isosurfaces of phase-averaged streamwise velocity ($\langle U\rangle/U_\infty = 0.9$, orange; $\langle U\rangle/U_\infty = 1.1$, green), for $St = 0.2$. Spanwise and panel-normal views are shown for each case. (a) $\phi = 45°$; (b) 60°; (c) 75°; (d) 105°; (e) 120°; (f) 135°. Each panel is moving into the negative y domain (phase angle 180°).

increasing Strouhal number. The changes in efficiency were calculated from curve fits applied to thrust and power. For concave panels, the efficiency is reduced by a maximum of about $\Delta\eta = 0.03$ compared to the square trailing edge case, while for convex panels the efficiency is improved by $\Delta\eta = 0.02$ for the case $\phi = 120°$ and $St = 0.4$. These are significant differences in that the average efficiency of the square panel is only about 0.1. The performance results

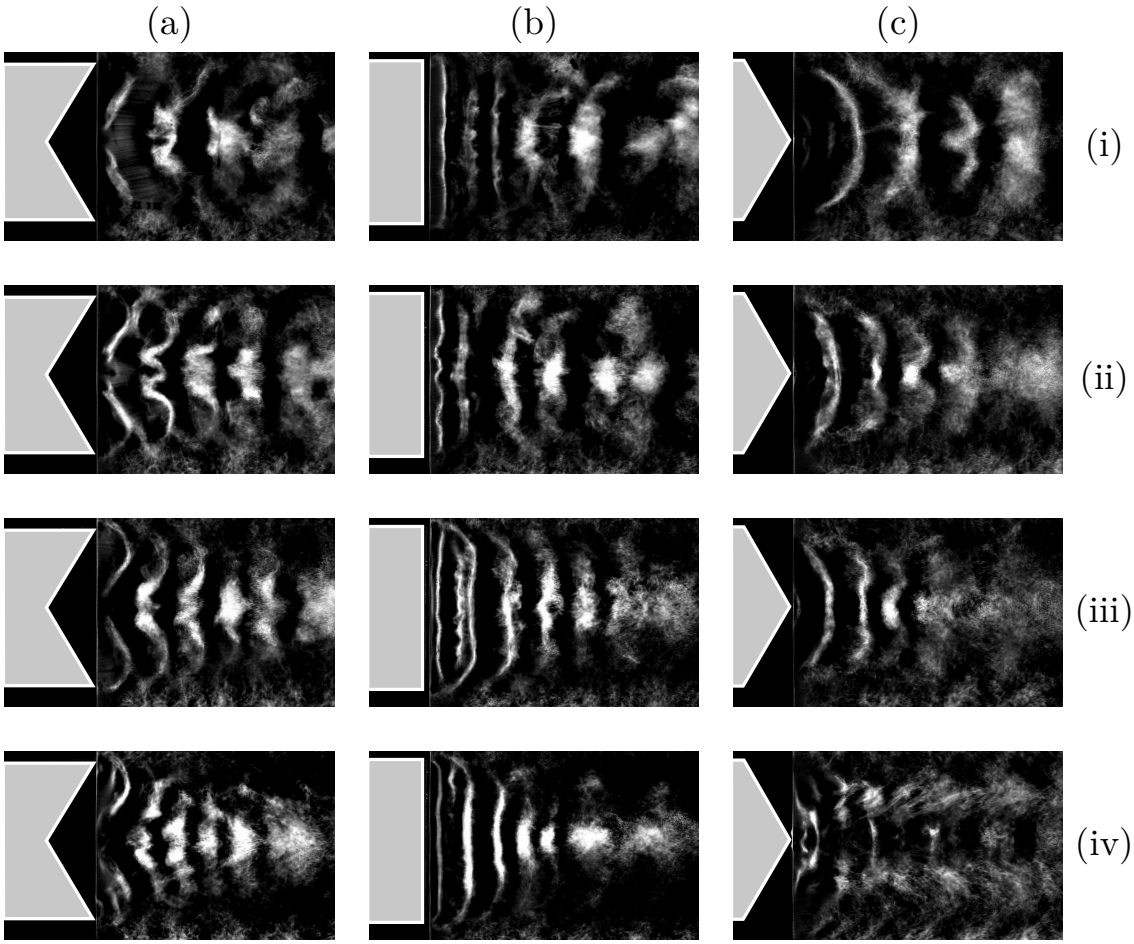

FIG. 8: Phase-averaged hydrogen bubble flow visualizations of the vortex structure for trailing edge angles (a) $\phi = 60°$; (b) 90°; and (c) 120°. The Strouhal number is fixed $St = 0.2$, but it is achieved using different pitch angle and frequency combinations: (i) $\theta = 4.3°$, $k = 8.36$; (ii) $\theta = 3.4°$, $k = 10.5$; (iii) $\theta = 2.85°$, $k = 12.57$; and (iv) $\theta = 2.3°$, $k = 15.71$. Videos available online (link to be added).

suggest that the quadfurcated wake is more efficient than the typical jet-like wake.

IV. DISCUSSION AND CONCLUSIONS

Rigid pitching panels with various trailing edge angles were experimentally studied, focusing on the panel wake and the propulsive performance. For the square panel the wake vortices underwent bending resulting in a wake compression. We showed that the angle of

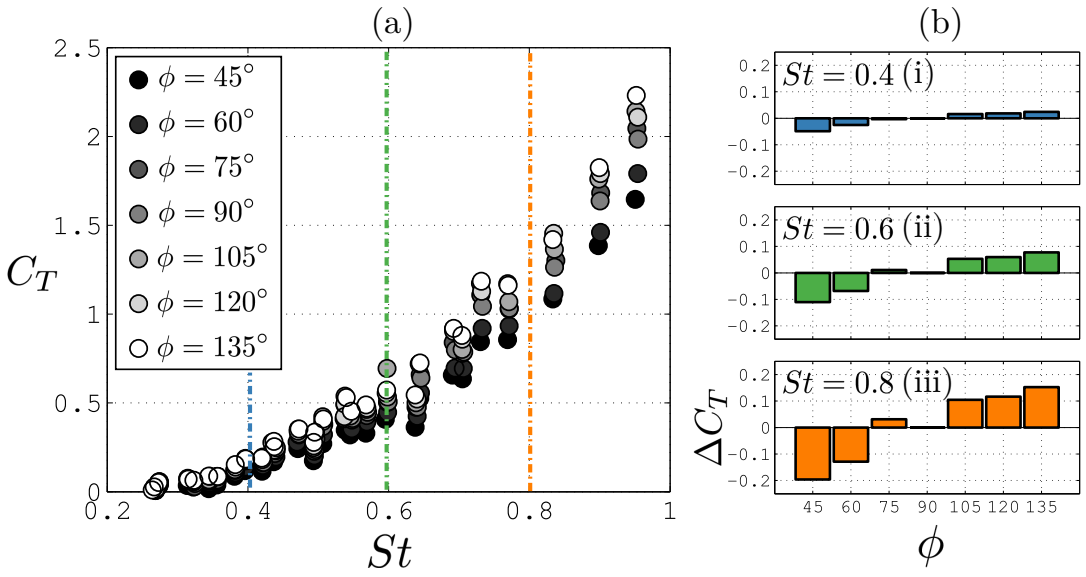

FIG. 9: (a) Thrust coefficient variation with Strouhal number. (b) Change in thrust coefficient relative to the square trailing edge case ($\phi = 90°$), for (i) $St = 0.4$; (ii) 0.6 (ii); (iii) 0.8.

the trailing edge bent the vortices such that the natural vortex bending and wake compression could be promoted (convex) or delayed (concave). This change in vortex formation had a significant impact on the time-averaged velocity field, with a single jet in the wake for the concave panels, and four jets for the convex panels. Hydrogen bubble flow visualization of the wake vortex structure supported the claims made from the PIV data.

Our data indicates that the thrust and efficiency of the panel generally improve with increasing trailing edge convexity, and concave trailing edges adversely affect performance. These performance modifications correspond to changes in the time-averaged wake. It should be emphasized that the three-dimensionality of the wake plays a crucial role in determining the panel performance. If wake measurements were restricted to the centerline plane, it would have seemed that the concave panel was producing a much stronger jet than the square and convex panels. In fact, the accelerated regions for convex panels move away from the center, and result in an overall increase in the momentum of the wake.

Finally, our results imply that the evolution of the various fish caudal fin shapes may be for other purposes than improving thrust and efficiency; most fish have concave tails, but our data suggests that this does not generate the optimum performance. It is possible that

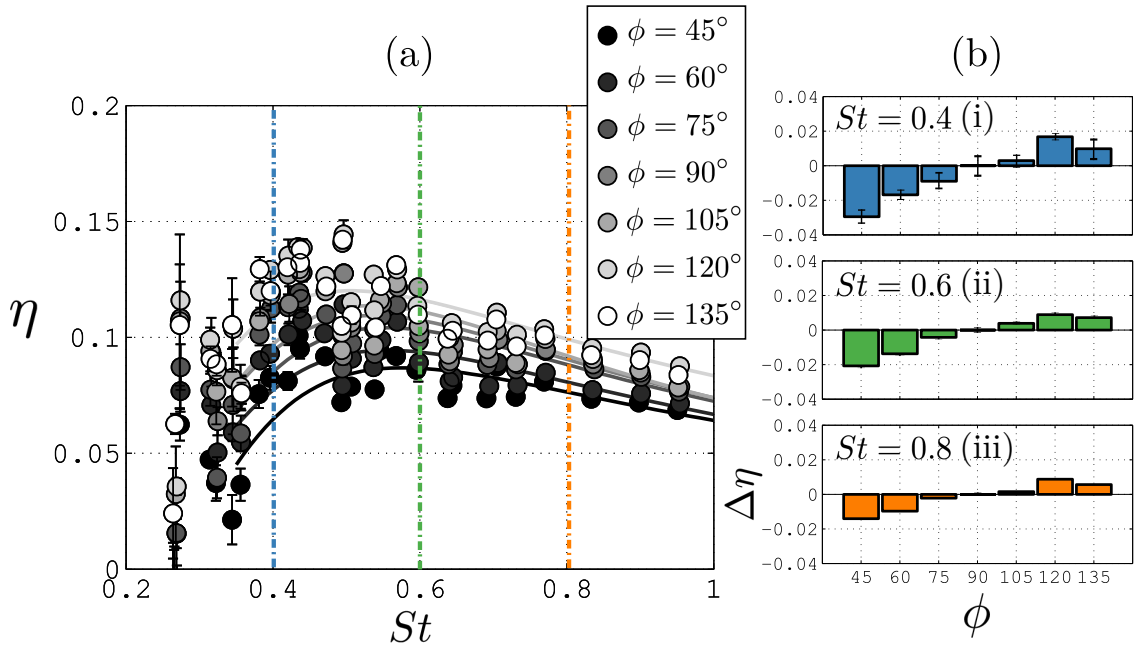

FIG. 10: (a) Efficiency variation with Strouhal number from the experimental data (symbols) and calculated by fitting power laws to the experimental thrust and power data (lines matching symbol color). (b) Change in efficiency relative to the square trailing edge case ($\phi = 90°$), for (i) $St = 0.4$; (ii) 0.6 (ii); (iii) 0.8.

the diversity in caudal fin trailing edge shape fulfills another evolutionary purpose, or it may be that trailing edge shape works together with another parameter to improve performance, for example, sweep angle. In any case, our observations are somewhat preliminary, in that Reynolds number, flexibility, and other forms of actuation (the addition of heave, for example), were not considered here.

This work was supported by the Office of Naval Research under MURI grant number N00014-14-1-0533 (program director Dr. Robert Brizzolara).

REFERENCES

[1]G. V. Lauder, "Function of the caudal fin during locomotion in fishes: kinematics, flow visualization, and evolutionary patterns," American Zoologist **40**, 101–122 (2000).

[2]V. Sambilay Jr, "Interrelationships between swimming speed, caudal fin aspect ratio and body length of fishes," Fishbyte **8**, 16–20 (1990).

[3]J. L. Sumich and J. F. Morrissey, *Introduction to the biology of marine life* (Jones & Bartlett Learning, 2004).

[4]G. Karpouzian, G. Spedding, and H. Cheng, "Lunate-tail swimming propulsion. part 2. performance analysis," Journal of Fluid Mechanics **210**, 329–351 (1990).

[5]M. Chopra, "Hydromechanics of lunate-tail swimming propulsion," Journal of Fluid Mechanics **64**, 375–392 (1974).

[6]G. Li, Z. Luodin, and X. Lu, "Numerical studies on locomotion perfromance of fish-like tail fins," Journal of Hydrodynamics, Ser. B **24**, 488–495 (2012).

[7]P. Liu and N. Bose, "Propulsive performance of three naturally occurring oscillating propeller planforms," Ocean Engineering **20**, 57–75 (1993).

[8]G. Lauder, J. Lim, R. Shelton, C. Witt, E. Anderson, and J. Tangorra, "Robotic models for studying undulatory locomotion in fishes," Marine Technology Society Journal **45**, 41–55 (2011).

[9]J. Buchholz and A. Smits, "On the evolution of the wake structure produced by a low-aspect-ratio pitching panel," Journal of Fluid Mechanics **546**, 433–443 (2006).

[10]M. Dhanak and B. Bernardinis, "The evolution of an elliptic vortex ring," Journal of Fluid Mechanics **109**, 189–216 (1981).

[11]M. Green, C. Rowley, and A. Smits, "The unsteady three-dimensional wake produced by a trapezoidal pitching panel," Journal of Fluid Mechanics **685**, 117–145 (2011).

[12]A. Sciacchitano, B. Wieneke, and F. Scarano, "PIV uncertainty quantification by image matching," Measurement Science and Technology **24**, 1–16 (2013).

[13]A. J. Smits and T. T. Lim, *Flow visualization: techniques and examples* (Imperial College Press, 2000).

[14]R. Kumar, J. King, and M. Green, "Momentum distribution in the wake of a trapezoidal pitching panel," Journal of Marine Technology Society **50** (2016).